# CONFORMAL-BASED SURFACE MORPHING AND MULTI-SCALE REPRESENTATION

KA CHUN LAM, CHENGFENG WEN AND LOK MING LUI

**Abstract.** This paper presents two algorithms, based on the conformal geometry, for the multi-scale representations of geometric shapes and surface morphing. A multi-scale surface representation aims to describe a 3D shape at different levels of geometric details, which allows analyzing or editing surfaces at the global or local scales effectively. Surface morphing refers to the process of interpolating between two geometric shapes, which has been widely applied to estimate or analyze deformations in computer graphics, computer visions and medical imaging. In this work, we propose two geometric models for surface morphing and multi-scale representation for 3D surfaces. The basic idea is to represent a 3D surface by its mean curvature function $H$ and conformal factor function $\lambda$, which uniquely determine the geometry of the surface according to Riemann surface theory. Once we have the $(\lambda, H)$ parameterization of the surface, post-processing of the surface can be done directly on the conformal parameter domain. In particular, the problem of multi-scale representations of shapes can be reduced to the signal filtering on the $\lambda$ and $H$ parameters. On the other hand, the surface morphing problem can be transformed to an interpolation process of two sets of $(\lambda, H)$ parameters. We test the proposed algorithms on 3D human face data and MRI-derived brain surfaces. Experimental results show that our proposed methods can effectively obtain multi-scale surface representations and give natural surface morphing results.

**Key words.** Surface morphing; Multi-scale representation; Conformal parameterization; Conformal factor; Mean curvature

**1. Introduction.** Mathematical geometry processing is an active research fields and has found important applications in different areas such as in computer visions, computer graphics and medical imaging. Surface morphing and multi-scale representations of 3D shapes are two important geometry processing problems. A multi-scale surface representation aims to describe a 3D shape at different levels of geometric details. Through a multi-scale representation of the surface, micro and macro geometric information can be extracted or represented in different scales, which allows analyzing or editing the surface at the global or local scales effectively. For example, in medical imaging, extracting feature landmarks from anatomical structures using different geometric quantities such as curvatures are important. Using the multi-scale representation of the surface, salient features can be extracted in both global and local levels of details. The extract features can provide a more comprehensive description of the anatomical structure [26, 27, 28]. Besides, most existing algorithms for surface registration require huge amount of computation cost [29, 30], which is impractical in medical imaging or computer visions. With the multi-scale representations of surfaces, one can easily obtain an approximated registration at the global scale and refine the registration at the local scale. This significantly speeds up of the computation and improves the accuracy of registering localized geometric details on surfaces [31, 32]. Surface morphing is another important topic in computer visions. Surface morphing refers to the process of interpolating between two geometric shapes, which has been widely applied to estimate or analyze deformations in computer graphics, computer visions and medical imaging. For example, surface morphing has been extensively applied to 3D computer animation production and video games [33]. By modeling gradual evolutionary changes of surfaces, we can smoothly transform one 3D surface into another and thus producing a continuous deformation of shape blending. Furthermore, applications of surface morphing for biological studies have also been widely studied. For example, morphing of anatomical structure like skeletons, organs or body movements are also essential for improving surgical visualization, medical

diagnosis and analysis. Therefore, developing effective algorithms to compute multi-scale representations of 3D surfaces and model shape evolution between surfaces are of utmost important.

Throughout this paper, we propose two geometric models for surface morphing and multi-scale representations for 3D surfaces using conformal geometry. According to Riemann surface theory, a Riemann surface can be uniquely determined by its conformal factor and mean curvature up to a rigid motion. Motivated by this, in this work, we represent the Riemann surface using its conformal factor function $\lambda$ and mean curvature function $H$ . The problem of finding the multi-scale representations and morphing of surfaces can be transformed to the $(\lambda, H)$ parameter domains. Given a Riemann surface $S$, its conformal factor $\lambda$ and mean curvature $H$ can be obtained easily through the conformal parameterization of the surface. Conversely, given $\lambda$ and $H$, we can reconstruct the corresponding Riemann surface by solving the natrual frame equations on the parameter domain. For the problem of multi-scale representations of shapes, once we obtain the $(\lambda, H)$ representation of the surface, a Fourier transform can be applied to $\lambda$ and $H$ separately and some filtering processes can be carried out on the Fourier coefficients. Once the filtered $(\tilde{\lambda}, \tilde{H})$ representation is obtained, we can restore a corresponding Riemann surface $\tilde{S}$ that best satisfies the Gauss-Codazzi and natural frame equations. A multi-scale representation of the surface can then be obtained. On the other hand, with the $(\lambda, H)$ representations of the surfaces, the surface morphing problem can be transformed to an interpolation process of two sets of $(\lambda, H)$ parameters. In particular, given two Riemann surfaces $S_1$ and $S_2$, instead of interpolating the coordinate functions of $S_1$ to $S_2$ directly, we propose to interpolate between $(\lambda_1, H_1)$ and $(\lambda_2, H_2)$ (which are the conformal factor and mean curvature representations of $S_1$ and $S_2$ respectively). The intermediate surfaces can then be reconstructed, which give a surface morphing between $S_1$ and $S_2$. To test the effectiveness of the proposed algorithms, we test the methods on 3D human face data and MRI-derived brain surfaces. Experimental results show that our proposed methods can effectively obtain multi-scale surface representations and give natural surface morphing results.

In short, the contributions of this paper are two-folded. First, we propose algorithms for obtaining the multi-scale representations of 3D surfaces by considering the representation of a Riemann surface using its conformal factor $\lambda$ and mean curvature $H$. By performing Fourier filtering on both $\lambda$ and $H$, our algorithm can effectively represent a surface in different scales of geometric details. Second, we propose an algorithm for morphing between two 3D surfaces using their corresponding $(\lambda, H)$ representation. As $\lambda$ and $H$ can fully describe the geometric information of the surfaces, a natural interpolation between two surfaces can be obtained through interpolating between the two sets of $(\lambda, H)$ representations. Experimental results show that the proposed morphing algorithm can produce natural surface morphing results effectively.

This paper is organized as follows. In Section 2, some related works will be reported. In Section 3, some basic mathematical background will be described. The proposed algorithms for surface morphing and multi-scale representations of shapes will be explained in details in Section 4. The numerical implementation details will be described in Section 5. We report the the experimental results in Section 6. The paper is summarized in Section 7.

**2. Previous work.** Conformal parameterization has been extensively studied [9, 10, 3, 4, 5]. For example, Hurdal et al. proposed to use circle packing for comput-

ing conformal parameterization and apply it to register human brain surfaces [8]. Gu et al. [3, 4, 5] proposed to compute conformal parameterization using harmonic energy minimization with holomorphic 1-forms and use it for brain surface registration. Authors in [1, 2] use a least square approach to find the conformal parameterization of surfaces, in which a free boundary parameterization will be result. By using conformal factor and curvatures, authors in [6, 7] proposed to use the shape index to measure geometric difference between hippocampal surfaces.

In computer visions, the multi-scale representations of shapes have also been widely used and studied. For example, the multi-scale representation has been applied in surface compression and progressive transmission [12, 13]. Multi-scale representations of shapes have also been effectively applied in shape analysis [14, 15], since the idea of multi-scale representation is to represent a surface with different scales of gemoetric details. For example, in [14], the authors proposed to construct a parameterization of a surface onto a simple domain, which is then used for remeshing and multi-resolution shape analysis. Cipriano et al. [16] proposed a localized shape descriptors that compactly characterize regions of a surface. The basic idea of these descriptors is to use a quadratic surface to fit the original surface. Multiscale representation has also been applied to 3D surface feature extraction [17]. The basic idea is to compute the shape index of a surface at multiple scales by fitting a surface to local neighborhood of different sizes. Maxima of surface variation, which is calculated by the variation of shape index, is chosen as the features of the 3D surfaces. Further applications of these features are used in surface registration. In computer graphics, multi-scale representation for point clouds has also been studied [18]. The authors suggested to first compute the point-based surface approximate at a coarser levels, followed by an application of geometric low pass filtering. This step is repeated successively to obtain a multi-scale representation.

Various algorithms for surface morphing, which tells us how a surface evolves, have been proposed. Liu et al. [19] proposed a modified as-rigid-as possible surface morphing algorithm for surface mesh evolution, which is originally proposed by Alexa [20]. Kanai et al. [21] first partition the original and target surfaces into pieces for constructing local parameterizations such that consistent meshes can be formed. In [22], a consistent surface controlling approach is proposed for shape optimization. By solving the optimization problem, the morphing problem is solved in the control space with some regularity and smoothness constraints. Morphing has also been applied in various fields. For example, in anatomical analysis, Rajamani et al. [23] proposed to construct a statistical model using Principal Component Analysis (PCA) through the training objects and by using weighted least square to fit the deformable model. A different approach to surface morphing is to create implicit functions for surfaces and apply a smooth interpolation between these implicit functions to construct the surface morphing. Hughes [24] proposed to transform the iso-surfaces of the models and interpolate between their corresponding Fourier transforms of the models. Turk et al. [25] combined both implicit function creation and interpolation steps to obtain the surface/volumes transformation.

**3. Mathematical background.** In this section, we describe some basic mathematical concepts relevant to our algorithms.

**3.1. Conformal factor and Curvature of a Riemann surface.** Recall that a Riemann surface $S$ is an oriented manifold of dimension two with a conformal structure. Locally every Riemann surfaces are Euclidean. Therefore, given two Riemann

surfaces $S_k$, $k = 1, 2$, they can be represented locally by

$$\phi_{S_k}(x_1, x_2) : U_k \in \mathbb{R}^2 \to S_k \in \mathbb{R}^3, \quad k = 1, 2 \tag{3.1}$$

The Riemannian metric on $S_k$ can then be written as

$$ds^2_{S_k} = \sum_{i,j} g^k_{i,j} dx^1 dx^2 \tag{3.2}$$

where

$$g^k_{i,j} = \frac{\partial \phi_{S_k}}{\partial x} \cdot \frac{\partial \phi_{S_k}}{\partial y}, \quad k = 1, 2 \tag{3.3}$$

With this local parameterization, for any given map $f : S_1 \to S_2$, $f$ can be represented locally by the coordinates $(x_1, x_2)$ as

$$\tilde{f} = \phi^{-1}_{S_2} \circ f \circ \phi_{S_1} : U_1 \to U_2. \tag{3.4}$$

Denote $\tilde{f} = (\tilde{f}_1, \tilde{f}_2)$ and let $v_1$ and $v_2$ be tangent vectors on $S_1$. By the mapping $f$, the tangent vectors can be mapped to $f_*(v_1)$ and $f_*(v_2)$ respectively. Using this new pair of tangent vectors, a new Riemannian metric $f^*(ds^2_{S_2})$ defined on $S_1$ can be induced by $f$ and $ds^2_{S_2}$:

$$\begin{aligned} f^*(ds^2_{S_2})(v_1, v_2) &:= < f_*(v_1), f_*(v_2) > \\ &= \sum_{i,j} g^2_{i,j} f_*(v_i) \cdot f_*(v_j) \\ &= \sum_{i,j} \left( \sum_{m,n} g^2_{mn} \frac{\partial \tilde{f}_i}{\partial x^m} \frac{\partial \tilde{f}_j}{\partial x^n} \right) v_i v_j \end{aligned} \tag{3.5}$$

With this new Riemannian metric, we say the map $f$ is conformal if

$$f^*(ds^2_{S_2}) = \lambda(x_1, x_2)^2 ds^2_{S_1} \tag{3.6}$$

where $\lambda(x_1, x_2)$ is called the conformal factor. Then for any parameterization $\varphi : S_1 = U \in \mathbb{R}^2 \to S_2$ satisfying the equation (3.6) is called a conformal parameterization. Intuitively, equation (3.6) tells us that a conformal map preserves the inner product of tangent vectors up to a scaling factor, which is the conformal factor $\lambda$. By using the properties of inner product, it can be shown that any conformal map preserves angles.

Another important geometric quantities is the curvature of a Riemann surface. Recall the mean curvature curvature $H$ is defined as the average of the principal curvatures:

$$H = \frac{k_1 + k_2}{2} \tag{3.7}$$

where $k_1$ and $k_2$ are the eigenvalues of the shape operator; the Gaussian curvature $K$ is defined as the product of the principal curvatures:

$$K = k_1 k_2 \tag{3.8}$$

If the conformal parameterization $\phi : U \in \mathbb{R}^2 \to S$ is given, the mean curvature $H$ and the Gaussian curvature $K$ can be computed using the conformal factor $\lambda$:

$$H = \frac{1}{2\lambda^2}\text{sign}(\phi)|\Delta\phi| \tag{3.9}$$

$$K = -\frac{1}{2\lambda^2}\Delta \log \lambda \tag{3.10}$$

where $\text{sign}(\phi) = \frac{<\Delta\phi,\vec{n}>}{|\Delta\phi|}$ and $\vec{n}$ is the unit surface normal.

Figure 3.1 shows the results of the conformal parameterization and the computation of $\lambda$ and $H$ of a typical MRI-derived brain surface. (a) shows the original brain surface mesh. (b) shows the conformal parameterization of the brain $U \in \mathbb{R}^2$. By defining texture coordinates with the conformal parameterization in (b), we synthesize a texture mapping onto the brain mesh as shown in (c). Note that small circles are preserved after the texture mapping, which is consistent with our intuitive understanding of a conformal parameterization: a conformal mapping maps infinitesimal circles to infinitesimal circles up to a scaling factor. Figure 3.1 (d) and (e) show the corresponding conformal factor $\lambda$ and mean curvature $H$ of the brain surface.

**3.2.** $(\lambda, H)$ **representation for surface.** Let $S$ be a Riemann surface embedded in $\mathbb{R}^3$. Since every Riemann surface is locally Euclidean, we can find $\phi(u, v)$ which parameterize $S$:

$$\phi(u, v) = (X(u, v), Y(u, v), Z(u, v)) \in \mathbb{R}^3 \tag{3.11}$$

Recall that the first and the second fundamental form are:

$$\begin{aligned} ds^2 &=< \phi_u, \phi_u > du^2 + 2 < \phi_u, \phi_v > dudv + < \phi_v, \phi_v > dv^2 \\ II &=< \phi_{uu}, \vec{n} > du^2 + 2 < \phi_u, \vec{n} > dudv + < \phi_{vv}, \vec{n} > v^2 \end{aligned} \tag{3.12}$$

where $\vec{n}$ is the unit surface normal.

Let $z = u + iv$ $(i = \sqrt{-1})$, $dz = du + idv$, $d\overline{z} = du - idv$ $\partial z = \frac{1}{2}\left(\frac{\partial}{\partial u} - i\frac{\partial}{\partial v}\right)$ and $\partial\overline{z} = \frac{1}{2}\left(\frac{\partial}{\partial u} + i\frac{\partial}{\partial v}\right)$. By assuming $\phi$ to be a conformal parameterization, we can rewrite the equations of natural frame $(\phi_z, \phi_{\overline{z}}, \vec{n})$ as:

$$\frac{\partial}{\partial z}\begin{pmatrix} \phi_z \\ \phi_{\overline{z}} \\ \vec{n} \end{pmatrix} = \begin{pmatrix} \frac{2}{\lambda}\lambda_z\phi_z + \mu\vec{n} \\ \frac{\lambda^2}{2}H\vec{n} \\ -H\phi_z - \frac{2\mu\phi_{\overline{z}}}{\lambda^2} \end{pmatrix} \tag{3.13}$$

where $\mu =< \phi_{zz}, \vec{n} >$. From equation (3.13), we know that $\phi$ can be determined by the conformal factor $\lambda$, mean curvature $H$, and $\mu$. Recall the Gauss-Codazzi equation:

$$\mu_{\bar{z}} = \frac{\lambda^2}{2}H_z \tag{3.14}$$

which can be further differentiated with respect to $z$ to obtain

$$\Delta\mu = \frac{1}{2}\lambda\left(2\lambda_z H_z + \lambda H_{zz}\right) \tag{3.15}$$

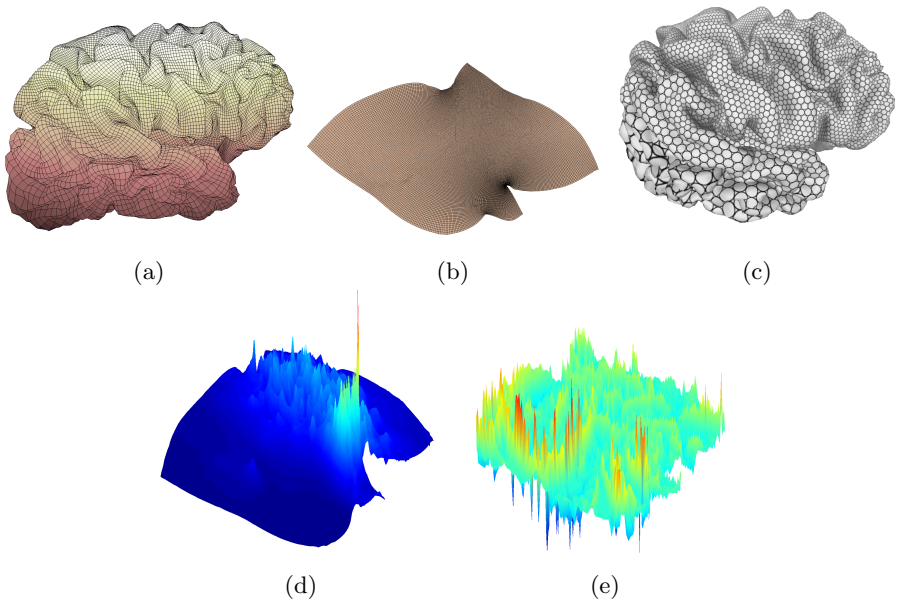


Fig. 3.1: Conformal Parameterization of a brain cortical surface. (a) shows the original brain mesh. (b) shows the conformal parameterization onto a rectangular conformal parameter domain in $\mathbb{R}^2$. We then texture the brain using the parameterization obtained from (b), as shown in (c). Note that conformal parameterization maps infinitesimal circles to circles. (d) and (e) show the conformal factor of the parameterization and the mean curvature of the brain surface respectively.

In other words, we can represent $\mu$ by the conformal factor $\lambda$ and $H$ as:

$$\mu = \frac{1}{2}\Delta^{-1}\left[\lambda\left(2\lambda_z H_z + \lambda H_{zz}\right)\right].$$

Therefore, given the Dirichlet boundary condition of $\phi$ on the neighbourhood $V$, we can obtain $\phi$ by solving the system of partial differential equation (3.13). As a consequence, given the boundary correspondence $\phi|_{\partial S}$, $S$ can be uniquely representation by the pair $(\lambda, H)$.

We summarize the above discussion as the following theorem.

THEOREM 1 ($(\lambda, H)$ representation). *Let $S$ be an open Riemann surface with ean curvature $H$. Let $\phi : U \in mathbbR^2$ be the conformal parameterization of $S$ with conformal factor $\lambda$. Suppose $V$ is a boundary neighborhood of $S$. Given the boundary value $\phi_{\partial V}$ of $\phi$, $S$ is uniquely determined by $\lambda$ and $H$.*

The $(\lambda, H)$ representation was proposed in [34] and applied for surface inpainting in [35].

**4. Methodology.** In this section, we propose two algorithms, which are the multi-scale representation algorithm and the surface morphing algorithm.

**4.1. Multi-scale representation of surfaces.** Given a surface $S$, our goal is to find a multi-scale representation of the surface that provides different scales of geometric details of the original surface. Instead of directly working on the coordinate

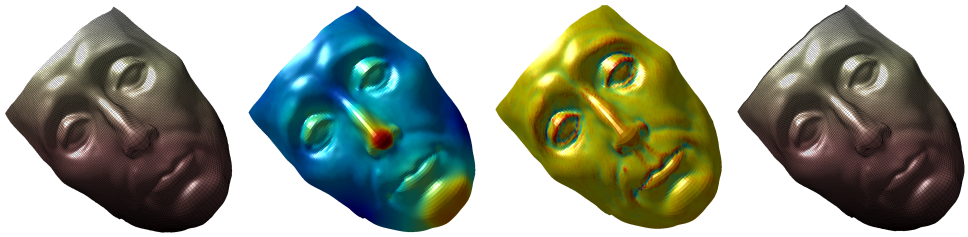

(a) (b) (c) (d)

Fig. 3.2: $(\lambda, H)$ representation of a human face. (a) shows the original mesh of a face. By finding the conformal parameterization of the human face to a rectangular conformal parameter domain in $\mathbb{R}^2$, we calculate the conformal factor, as shown in (b). (c) shows the mean curvature of the human face. By using $\lambda$ and $H$, we can reconstruct the human face as shown in (d).

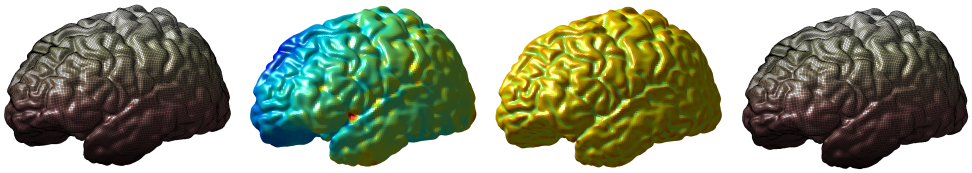

(a) (b) (c) (d)

Fig. 3.3: $(\lambda - H)$ representation of a human brain. (a) shows the original mesh of a brain. By finding the conformal parameterization of the brain to a rectangular conformal parameter domain, we calculate the conformal factor, as shown in (b). (c) shows the mean curvature of the brain. By using $\lambda$ and $H$, we can reconstruct the brain as shown in (d).

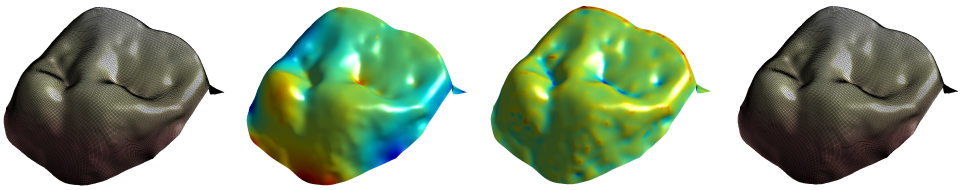

(a) (b) (c) (d)

Fig. 3.4: $(\lambda, H)$ representation of a human tooth. (a) shows the original mesh of a tooth. By finding the conformal parameterization of the tooth to a rectangular conformal parameter domain, we calculate the conformal factor, as shown in (b). (c) shows the mean curvature of the tooth. By using $\lambda$ and $H$, we can reconstruct the tooth as shown in (d).

functions of the surface embedded in $\mathbb{R}^3$, our proposed algorithm considers the $(\lambda, H)$ representation of the surface. We first obtain a rectangular conformal parameterization $U = [-T_1, T_1] \times [-T_2, T_2] \in \mathbb{R}^2$ of the surface $S$. By using equations 3.6 and 3.9,

we can calculate the corresponding $\lambda$ and $H$ of the surface $S$. By viewing different scales of geometric details as different scales of noises, the main idea of our algorithm is to apply the traditional denoising method on the geometric quantities $\lambda$ and $H$ to find the multi-scale representation of the surface. In other words, for a specific scale $K$, we first apply Fourier transform on $\lambda$ and $H$ respectively in $U$ to obtain two sets of Fourier coefficients $C^{\lambda}$ and $C^{H}$:

$$C^{\lambda}_{m,n} = \frac{1}{4\pi}\int_{-T_2}^{T_2}\int_{-T_1}^{T_1} \lambda(x,y)e^{-i\pi jx/T_1}e^{-i\pi ky/T_2}dxdy \tag{4.1}$$

$$C^{H}_{m,n} = \frac{1}{4\pi}\int_{-T_2}^{T_2}\int_{-T_1}^{T_1} H(x,y)e^{-i\pi jx/T_1}e^{-i\pi ky/T_2}dxdy \tag{4.2}$$

where the original $\lambda$ and $H$ can be expressed by the Fourier expansion as follows:

$$\lambda(x,y) = \sum_{m,n-\infty}^{\infty} C^{\lambda}_{m,n}e^{i\pi mx/T_1}e^{j\pi ny/T_2} \tag{4.3}$$

$$H(x,y) = \sum_{m,n-\infty}^{\infty} C^{H}_{m,n}e^{i\pi mx/T_1}e^{j\pi ny/T_2} \tag{4.4}$$

Treating like denoising white noise in signal processing, we consider coefficients with magnitude smaller than $K$ as pure noise and set them to zero. The corresponding truncated Fourier expansions of $\lambda$ and $H$ form a new pair of denoised $(\tilde{\lambda}, \tilde{H})$ parameterization, which represents a "denoised" surface with some of the geometric details removed. Using the $(\lambda, H)$ reconstruction scheme, we can get the corresponding surface $\tilde{S}$ of scale $K$ as required.

In summary, the proposed multi-scale representation algorithm can be described as follows:

**Algorithm 1:** Multi-scale representation of a surface

**Input**: Surface $S$, Scale $K$
**Output**: Surface $\tilde{S}$ of scale $K$

1. Conformally parameterize $S$ into $U = [-T_1, T_1] \times [-T_2, T_2] \in \mathbb{R}^2$;
2. Compute conformal factor $\lambda$ and mean curvature $H$;
3. Apply Fourier transform on $\lambda$ and $H$ to get $C^{\lambda}_{m,n}$ and $C^{H}_{m,n}$ respectively;
4. Truncate the Fourier coefficients less than the bound $K$ to obtain $\tilde{C}^{\lambda}_{m,n}$, $\tilde{C}^{H}_{m,n}$;
5. Apply inverse Fourier transform to get $\tilde{\lambda}$ and $\tilde{H}$;
6. Carry out $(\lambda, H)$ reconstruction scheme to get $\tilde{S}$ of scale $K$.

**4.2. Surface Morphing.** Given two surfaces $S_1$ and $S_2$, the process of finding the evolution from surface $S_1$ to $S_2$ is called surface morphing. In other words, our goal is to compute every $S(t)$, where $t \in [0,1]$, $S(0) = S_1$ and $S(1) = S_2$. To

achieve this, we again consider the $(\lambda, H)$ representation rather than the $\mathbb{R}^3$ space directly. Let $\partial S_i$ be the boundary of surface $S_i$, $i = 1, 2$. By assuming that we already have the boundary matching obtained from arc-length parameterization or some other curve matching algroithms [36], we interpolate every points on $\partial S_1$ linearly in $\mathbb{R}^3$ to corresponding points in $\partial S_2$:

$$\begin{pmatrix} x(t) \\ y(t) \\ z(t) \end{pmatrix} = (1-t) \begin{pmatrix} x_1 \\ y_1 \\ z_1 \end{pmatrix} + t \begin{pmatrix} x_2 \\ y_2 \\ z_2 \end{pmatrix} \tag{4.5}$$

where $(x_1, y_1, z_1)^T \in \partial S_1$ and $(x_2, y_2, z_2)^T \in \partial S_2$. From this, we obtain a simple boundary morphing approximation from surface $S_1$ to $S_2$. Next, we compute rectangular conformal parameterization for both surface $S_1$ and $S_2$ respectively as in Algorithm 1. Two pairs $(\lambda_1, H_1)$ and $(\lambda_2, H_2)$ corresponding to surface $S_1$ and $S_2$ can then be obtained. To approximate the evolution naturally, we propose to morph the geometric quantities $\lambda$ and $H$ from the pair $(\lambda_1, H_1)$ to $(\lambda_2, H_2)$ by simply linear interpolation:

$$\lambda(t) = (1-t)\lambda_1 + t\lambda_2 \tag{4.6}$$

$$H(t) = (1-t)H_1 + tH_2 \tag{4.7}$$

Substituting $t \in [0, 1]$ with different values, we get a sequence of pairs $(\lambda(t), H(t))$ with boundary constraint $\partial S(t)$. By using $(\lambda, H)$ reconstruction algorithm, the corresponding surface $S(t)$, which best fits the Gauss Codazzi and natural frame equations, can be constructed. This gives a morphing surface at time $t \in [0, 1]$.

Our proposed morphing algorithm can be summarized as follows:

**Algorithm 2:** Morphing of surfaces

**Input**: Surface $S_1$ and $S_2$, Time $t$
**Output**: Intermediate surface $S(t)$ between $S_1$ and $S_2$

1 Obtain the boundary matching between $S_1$ and $S_2$;
2 Compute the boundary morphing $\partial S(t)$ by linear interpolation pointwisely;
3 Compute conformal parameterization for both $S_1$ and $S_2$;
4 Compute $(\lambda_1, H_1)$ and $(\lambda_2, H_2)$ corresponding to $S_1$ and $S_2$ respectively;
5 Use the $(\lambda, H)$ reconstruction algorithm with $(\lambda(t), H(t))$ and $\partial S(t)$ to compute $S(t)$.

**5. Numerical algorithms.** In this section, we discuss the numerical implementation of the algorithms we proposed in this paper. Firstly, we will briefly describe how we obtain the $(\lambda, H)$ representation and the implementation of the reconstruction scheme of the surface $S$ with given conformal factor $\lambda$ and mean curvature $H$. Secondly, we will explain how the algorithms for multi-scale representation and surface morphing proposed in previous section can be implemented.

**5.1. Numerical implementation of $(\lambda, H)$ representation and surface reconstruction.** We basically follows the numerical implementation in [35]. Given a surface $S$, the conformal parameterization can be obtained by using some well-established conformal parameterization algorithms [3, 4, 5, 8, 10]. By applying the algorithm proposed in [11], we obtain the rectangular conformal parameterization $U = [0,1] \times [0,T] \in \mathbb{R}^2$ of the surface $S$. Denote the discretized parameterization domain $U$ to be

$$U_{ij} = (ih, Tjh), \quad h = \frac{1}{N},\ 0 \leq i \leq N,\ 0 \leq j \leq N \tag{5.1}$$

Correspondingly, we have

$$\phi_{ij} = \phi(U_{ij}) \quad H_{ij} = H(U_{ij}) \quad \text{and} \quad \lambda_{ij} = \lambda(U_{ij}) \tag{5.2}$$

To obtain the conformal factor $\lambda_{ij}$, recall that a conformal parameterization $\phi$ preserves the first fundamental form up to conformal factor. Therefore we can approximate the discrete conformal factor $\lambda_{ij}$ by

$$\begin{aligned} \lambda_{ij} =& < \frac{\partial \phi(U_{ij})}{\partial z}, \frac{\partial \phi(U_{ij})}{\partial \bar{z}} > \\ \approx& \frac{1}{2}\left[\left|\frac{\phi_{i+1,j} - \phi_{i-1,j}}{2h}\right|^2 + \left|\frac{\phi_{i,j+1} - \phi_{i,j-1}}{2h}\right|^2\right] \end{aligned} \tag{5.3}$$

For the mean curvature $H_{ij}$, we consider equation (3.9):

$$H_{ij} = H(U_{ij}) = \frac{1}{2\lambda_{ij}} \text{sign}(\phi_{ij}) |\Delta \phi_{ij}| \tag{5.4}$$

where we approximate

$$\Delta \phi_{ij} = \frac{\phi_{i+1,j} + \phi_{i-1,j} - 4\phi_{i,j} + \phi_{i,j+1} + \phi_{i,j-1}}{h^2} \tag{5.5}$$

$$\text{sign}(\phi_{ij}) = \text{sign}\left(< \Delta \phi_{ij}, \vec{n_{ij}} >\right) \tag{5.6}$$

$$\vec{n_{ij}} = \left(\frac{\phi_{i+1,j} - \phi_{i-1,j}}{2h}\right) \times \left(\frac{\phi_{i,j+1} - \phi_{i,j-1}}{2h}\right) / \left\| \left(\frac{\phi_{i+1,j} - \phi_{i-1,j}}{2h}\right) \times \left(\frac{\phi_{i,j+1} - \phi_{i,j-1}}{2h}\right) \right\| \tag{5.7}$$

If we are given the $(\lambda, H)$ representation, we can reconstruct the surface $S$ by solving equation (3.13). Let $((\phi_z)_{ij}, (\phi_{\bar{z}})_{ij}, \vec{n}_{ij}) = (P_{ij}, Q_{ij}, N_{ij})$ be the natural frame at $U_{ij}$. Similar to above, we can discretize the system into the following:

$$\frac{1}{2h}\begin{pmatrix} (P_{i+1,j} - P_{i-1,j}) - \sqrt{-1}(P_{i,j+1} - P_{i,j-1}) \\ (Q_{i+1,j} - Q_{i-1,j} - \sqrt{-1}(Q_{i,j+1} - Q_{i,j-1}) \\ 2hN_{ij} \end{pmatrix} = \begin{pmatrix} \frac{2}{\lambda_{ij}}(\lambda_z)_{ij} P_{ij} + \mu_{ij} N_{ij} \\ \frac{\lambda_{ij}^2}{2} H_{ij} N_{ij} \\ -H_{ij} P_{ij} - \frac{2\mu_{ij} Q_{ij}}{\lambda_{ij}^2} \end{pmatrix} \tag{5.8}$$

We solve Equation (5.8) by the least-square method.
Once we obtain $(P_{ij}, Q_{ij}, N_{ij})$ by solving equation (5.8), we can reconstruct the surface by solving

$$\frac{1}{2h}\begin{pmatrix} \phi_{i+1,j} - \phi_{i-1,j} \\ \phi_{i,j+1} - \phi_{i,j-1} \end{pmatrix} = \begin{pmatrix} (P_{ij} + Q_{ij})/2 \\ \sqrt{-1}(P_{ij} - Q_{ij})/2 \end{pmatrix} \tag{5.9}$$

**5.2. Numerical implementation of multi-scale representation of surface.** Given a surface $S$, Algorithm 1 produces a surface $\tilde{S}$ with a coarser scale of geometric details. Since we have chosen the conformal parameterization domain $U$ to be a rectangle, conformal factor $\lambda$ and mean curvature $H$ are well defined on $U$ as well. Then by using Discrete Fast Fourier transform (DFT), we are able to get $C_{ij}^{\lambda}$ and $C_{ij}^{H}$ immediately. The trucation process is simply by

$$\begin{aligned} C_{ij}^{\lambda} &= 0 \quad \text{if} \quad \left|C_{ij}^{\lambda}\right| \leq K; \\ C_{ij}^{H} &= 0 \quad \text{if} \quad \left|C_{ij}^{H}\right| \leq K. \end{aligned} \tag{5.10}$$

By using Inverse Discrete Fast Fourier transform (IDFT) on the updated $C_{ij}^{\lambda}$ and $C_{ij}^{H}$, $(\tilde{\lambda}, \tilde{H})$ can be obtained.

**5.3. Numerical implementation of surface morphing.** In Algorithm 2, there are many ways to obtain meaningful boundary registration result. Here we discuss the method of arc-length parameterization for boundary matching that works very well as shown in our experimental results in the next section.

Given two surfaces $S_1$ and $S_2$ with boundaries $\partial S_1$ and $\partial S_2$, denotes the vertices on boundaaries to be $\{v_1(k)\}_k$ and $\{v_2(h)\}_h$ respectively. We assume we have labelled few point-correspondences:

$$v_1(p_i) = v_2(q_i), \quad 1 \leq p_i \leq I, \quad I \leq q_i \leq J, \quad i = 1 : N \tag{5.11}$$

Consider the line segments $[v_1(p_i), v_1(p_i+1), ..., v_1(p_{i+1})] \subset \{v_1(k)\}_k \subset \mathbb{R}^3$ and $[v_2(q_i), v_2(q_i+1), ..., v_2(q_{i+1})] \subset \{v_2(h)\}_h \subset \mathbb{R}^3$, two arc-length parameterization $(\alpha, f_1(\alpha))$ and $(\beta, f_2(\beta))$ can be obtained, where $p_i \leq \alpha \leq p_{i+1}$, $q_i \leq \beta \leq q_{i+1}$, $f_1(\alpha) = v_1(\alpha)$ and $f_2(\beta) = v_2(\beta)$ respectively. To obtain the boundary registration, we define $P(\alpha)$ as:

$$P(\alpha) = f_2\left(q_i + (q_{i+1} - q_i)\frac{\alpha - p_i}{p_{i+1} - p_i}\right) \tag{5.12}$$

where $P(\alpha) \in \mathbb{R}^3$. By substituting $\alpha$ such that $p_i \leq \alpha \leq p_{i+1}$, we can obtain the corresponding position of each $v_1(\alpha) \in \{v_1(k)\}_k$ on $\partial S_2$.

**6. Experimental results.** We have tested our multi-scale algorithm and morphing algorithm on both synthetic data and real medical data. In the following subsections, experimental results of the proposed algorithms are reported.

**6.1. Surface reconstruction.** Our proposed algorithms depend on the $(\lambda, H)$ representations of the Riemann surfaces. To examine how effective and accurate this geometric representation can represent the surface, we consider the $(\lambda, H)$ representation of a human face, a brain cortical surface and a teeth surface. Figure 3.2(a) shows the original human face. We parameterize the surface onto the 2D rectangular conformal parameter domain and compute the conformal factor. The conformal factor is visualized as the colormap on the surface, which is shown in (b). The mean curvature of the surface is shown in (c). The conformal factor and mean curvature determine the surface. In (d), we reconstruct the surface from the conformal factor and mean curvature. Note that the surface closely resembles to the original surface in (a). We

also examine the $(\lambda, H)$ representations for the brain cortical surface and the teeth surface as shown in Figure 3.3 and Figure 3.4. Again, the $(\lambda, H)$ representations can accurately represent the surfaces. From the $(\lambda, H)$ representations, the surfaces can be reconstructed, which closely resemble to the original surfaces.

**6.2. Multi-scale representation of surfaces.** We first test our proposed surface multi-scale representation algorithm on a synthetic human surface. Figure 6.1 (a) shows the original surface mesh of a human face model. Using Algorithm 1, we compute different levels of geometric details as shown in (b) – (f). The approximation levels decrease from (b) to (f) by increasing the bound $K$ in the algorithm. In other words, we truncated more and more terms in the Fourier expansion of both $\lambda$ and $H$. Therefore, facial characteristics like eyes, nose and mouth are fading gradually.

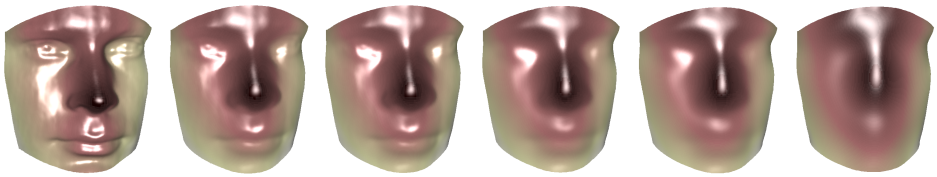

(a) (b) (c) (d) (e) (f)

Fig. 6.1: Result of the multi-scale representation of a human face surface. (a) shows the original human face. (b)-(f) show the multi-scale representation of the face obtained from the proposed algorithm. The approximation levels of the multi-scale representation decreases from the fine-scale (See (b)) to the coarse-scale (See (f)). Note that through (b) to (f), facial characteristics such as eyes, nose and mouth are fading out. This is consistent with our algorithm, which coarsens the $(\lambda, H)$ representation throughout the process.

We have also tested our multi-scale algorithm on a human brain surface, which has a more complicated surface geometric structure. Figure 6.2 (a) shows the original brain surface. There are lots of different sizes and lengths of sulcal located on the brain surface. By applying Algorithm 1 to the brain surface, we obtain the multi-scale representation as shown in (b) – (i). Similarly, the approximation levels decreases from (b) to (i) by increasing the bound $K$ in Algorithm 1. Note that through (b) to (i), geometric features like the sulci are fading out. This is consistent with our reduction in the number of effective Fourier coefficients. This also shows that our algorithm work well on complicated surfaces and provide a multi-scale representation of different surfaces.

**6.3. Surface Morphing.** We have tested our algorithm for morphing from one surface $S_1$ to another surface $S_2$ according to the $(\lambda, H)$ representation. Figure 6.3 shows the synthetic human faces of a man (a) and a woman (f). We first obtain their corresponding $(\lambda, H)$ representation $(\lambda_1, H_1)$ and $(\lambda_2, H_2)$ and their boundary correspondence. Then we approximate the surface evolution by linearly interpolating the $(\lambda, H)$ representation between them. From this, we can get a sequence of pairs $(\lambda(t), H(t))$ which approximate the morphing from surface $S_1$ to $S_2$. With these sequences of $(\lambda, H)$ representation, we reconstruct the corresponding surfaces as shown in Figure 6.3 (b)–(e). Experimental result shows that the proposed algorithm can produce a natural morphing between different surfaces by simply interpolate the ge-

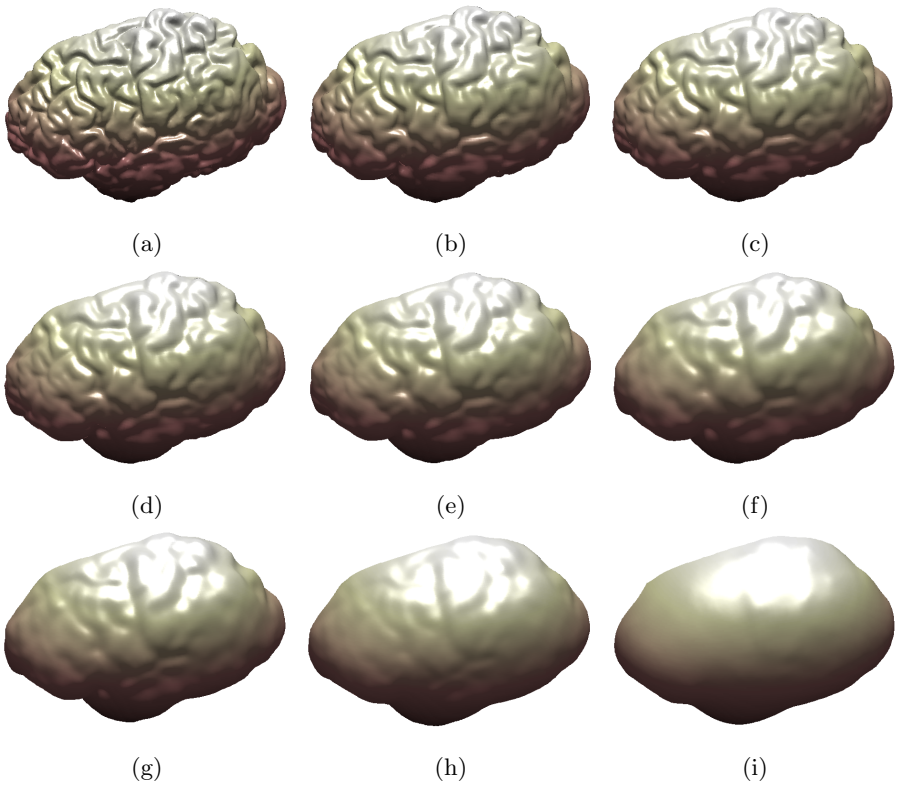


Fig. 6.2: Result of the multi-scale representation of a brain surface. (a) shows the original brain surface. (b)-(i) show the multi-scale representation of the brain obtained from the proposed algorithm. The approximation levels of the multi-scale representation decreases from the fine-scale (See (b)) to the coarse-scale (See (i)). Note that through (b) to (i), geometric characteristics like sulci on the brain are fading out. This is consistent with our algorithm which coarsens the $(\lambda, H)$ representation throughout the process.

ometric quantities $\lambda$ and $H$ that can fully describe the surfaces.

We also test our morphing algorithm to interpolate between two teeth surfaces. Figure 6.4 (a) and (f) show the two human teeth surfaces. By using Algorithm 2, we interpolate $\lambda$ and $H$ and reconstruct the corresponding surfaces from the $(\lambda, H)$ representation as shown in (b) – (e). Notice that by using the proposed morphing algorithm, surface features like local valley and ridges can natural deformed as both are described by the mean curvature and conformal factor. Therefore, our proposed algorithm produces good morphing approximation, which follows the geometry of the two surfaces.

**7. Conclusions.** This paper presents two novel algorithms for computing the multiscale representation of a surface and morphing between two surfaces. Instead of directly tackling the problems with the coordinate functions of the surfaces, we adopt the $(\lambda, H)$ representation proposed earlier in [34][35]. By the Riemann surface theory, given any surface $S$, we can find the conformal factor $\lambda$ and mean curvature $H$, which

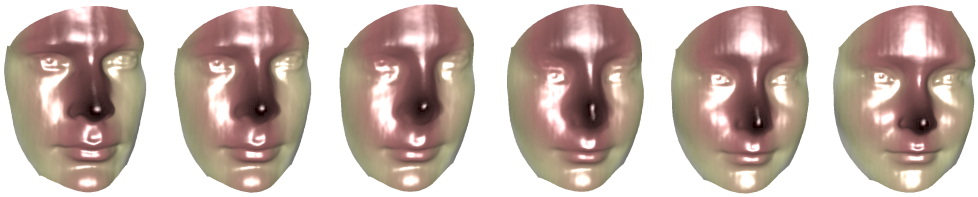

(a) (b) (c) (d) (e) (f)

Fig. 6.3: Surface morphing between two human faces (from a man face to a woman face) using the $(\lambda, H)$ representations. (a) and (f) show a man and a woman face respectively. By using the morphing algorithm, we interpolate $\lambda$ and $H$ and reconstruct the corresponding surface from the $(\lambda, H)$ representation. (b) – (e) shows the morphing results.

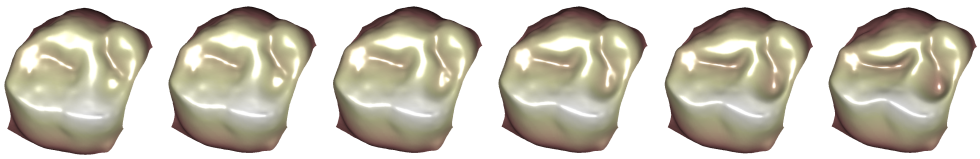

(a) (b) (c) (d) (e) (f)

Fig. 6.4: Surface morphing between two teeth using $(\lambda, H)$ representative. (a) and (f) show Tooth 1 and Tooth 2 respectively. By using the morphing algorithm, we interpolate $\lambda$ and $H$ and reconstruct the corresponding surface from the $(\lambda, H)$ representation. (b) – (e) shows the morphing results. Note that a natural evolution of ridges and valleys from Tooth 1 to Tooth 2 are obtained.

uniquely determine the surface $S$. By using the $(\lambda, H)$ representation, the problem of multi-scale representation is transformed to a signal processing problem of both geometric quantities $\lambda$ and $H$. In other words, by treating the geometric quantlties $\lambda$ and $H$ as signals, we can extract different scales of geometric details from the surface through the surface reconstruction from the truncated $(\lambda, H)$ representation.

Moreover, a surface morphing algorithm has also been proposed in this work. We consider to approximate the deformation of surfaces through their corresponding $(\lambda, H)$ representations. To morph between two surfaces, we propose to linearly interpolate between the $(\lambda, H)$ representations of the two surfaces. Since conformal factor and mean curvature can fully describe the geometric characteristics of the surface, our algorithm can effectively compute a natural morphing between two surfaces, as shown in the experimental results.

Note that our algorithms work on simply-connected open surfaces. In the future, we will consider extending our proposed algorithms on genus zero closed surfaces by making use of the spherical harmonic expansion and spherical harmonic conformal mapping. We will also consider to extend our algorithms to point clouds.

**Acknowledgements.** Lok Ming Lui is supported by CUHK Focus Investment Scheme (Project ID: 1902036) and RGC GRF (Project ID: 2191010).

REFERENCES


1. Lévy B., Petitjean S., Ray N., Maillot J. Least squares conformal maps for automatic texture atlas generation. *ACM Trans Graph* **2002**, *21*, 362–371.
2. Desbrun M., Meyer M., Alliez P. Intrinsic parameterizations of surface meshes. *Proceedings of Eurographics* **2002**, 209–218.
3. Gu, X., Wang, Y., Chan, T. F., Thompson, P. M., & Yau, S. T. Genus zero surface conformal mapping and its application to brain surface mapping. *Information Processing in Medical Imaging* **2003**, 172–184.
4. Wang, Y., Lui, L. M., Gu, X., Hayashi, K. M., Chan, T. F., Toga, A. W., & Yau, S. T. Brain surface conformal parameterization using Riemann surface structure. *Medical Imaging, IEEE Transactions* **2007**, *26(6)*, 853–865.
5. Gu, X., & Yau, S. T. Computing conformal structure of surfaces. *arXiv preprint cs/0212043* **2002**.
6. Lui, L. M., Wong, T. W., Zeng, W., Gu, X., Thompson, P. M., Chan, T. F., & Yau, S. T. Optimization of surface registrations using beltrami holomorphic flow. *Journal of Scientific Computing* **2012**, *50(3)*, 557–585.
7. Lui, L. M., Wong, T. W., Thompson, P., Chan, T., Gu, X., & Yau, S. T. Shape-based diffeomorphic registration on hippocampal surfaces using beltrami holomorphic flow. *Medical Image Computing and Computer-Assisted InterventionMICCAI* **2010** , 323–330.
8. Hurdal, M. K., & Stephenson, K. Discrete conformal methods for cortical brain flattening. *Neuroimage* **2009**, *45(1)*, S86-S98.
9. Fischl, B., Sereno, M. I., Tootell, R. B., & Dale, A. M. High-resolution intersubject averaging and a coordinate system for the cortical surface. *Human brain mapping* **1999**, *8(4)*, 272–284.
10. Haker, S., Angenent, S., Tannenbaum, A., Kikinis, R., Sapiro, G., & Halle, M. Conformal surface parameterization for texture mapping. *Visualization and Computer Graphics, IEEE Transactions* **2000**, *6(2)*, 181–189
11. Lui, L. M., Lam, K. C., Wong, T. W., & Gu, X. Texture map and video compression using Beltrami representation. *SIAM Journal on Imaging Sciences* **2013**, **6(4)**, 1880–1902.
12. Khodakovsky, A., Schroder, P., & Sweldens, W. Progressive geometry compression. *Proceedings of the 27th annual conference on Computer graphics and interactive techniques* **2000**, 271–278.
13. Peyré, G., & Mallat, S. Surface compression with geometric bandelets. *ACM Transactions on Graphics (TOG)* **2005**, *24(3)*, 601–608.
14. Eck, M., DeRose, T., Duchamp, T., Hoppe, H., Lounsbery, M., & Stuetzle, W. Multiresolution analysis of arbitrary meshes. *Proceedings of the 22nd annual conference on Computer graphics and interactive techniques*, **1995**, 173–182.
15. Gross, M. H., & Hubeli, A. Eigenmeshes. *Tech. rep., Department of Computer Science, ETH Zurich* **2000**.
16. Cipriano, G., Phillips, G. N., & Gleicher, M. Multi-scale surface descriptors. *Visualization and Computer Graphics, IEEE Transactions* **2009**, *15(6)*, 1201–1208.
17. Ho, H. T., & Gibbins, D. Multi-scale feature extraction for 3d surface registration using local shape variation. *Image and Vision Computing New Zealand, 2008. IVCNZ 2008. 23rd International Conference. IEEE.* **2008**, 1–6.
18. Pauly, M., Kobbelt, L. P., & Gross, M. Point-based multiscale surface representation. *ACM Transactions on Graphics (TOG)* **2006**, 25(2), 177–193.
19. Liu, Y. S., Yan, H. B., & Martin, R. R. As-Rigid-As-Possible Surface Morphing. *Journal of Computer Science and Technology* **2011**, *26(3)*, 548–557.
20. Alexa, M., Cohen-Or, D., & Levin, D. As-rigid-as-possible shape interpolation. *Proceedings of the 27th annual conference on Computer graphics and interactive techniques* **2000**, 157–164.
21. Kanai, T., Suzuki, H., & Kimura, F. Three-dimensional geometric metamorphosis based on harmonic maps. *The Visual Computer* **1998**, *14(4)*, 166–176.
22. Hojjat, M., Stavropoulou, E., & Bletzinger, K. U. The vertex morphing method for node-based shape optimization.*Computer Methods in Applied Mechanics and Engineering* **2014**, 268, 494–513.
23. Rajamani, K. T., Ballester, M. A. G., Nolte, L. P., & Styner, M. A novel and stable approach to anatomical structure morphing for enhanced intraoperative 3D visualization. *Medical Imaging* **2005**, 718–725.
24. Hughes, J. F. Scheduled Fourier volume morphing. *ACM SIGGRAPH Computer Graphics* **1992**, *26(2)*, 43–46.
25. Turk, G., & O'Brien, J. F. Shape transformation using variational implicit functions. *ACM*

*SIGGRAPH 2005 Courses* **2005** *13*.
26. Yuen, P. C. Multi-scale representation and recognition of three dimensional surfaces using geometric invariants. *Doctoral dissertation, University of Surrey* 2001.
27. Pauly, M., Keiser, R., & Gross, M. Multi-scale Feature Extraction on Point Sampled Surfaces. *Computer graphics forum* **2003** *22(3)*, 281–289.
28. Fadaifard, H., & Wolberg, G. Multiscale 3D feature extraction and matching. *3D Imaging, Modeling, Processing, Visualization and Transmission (3DIMPVT)* **2011**, 228–235.
29. Vaillant, M., & Glaunes, J. Surface matching via currents. *Information Processing in Medical Imaging* **2005**, 381–392.
30. Yeo, B. T., Sabuncu, M. R., Vercauteren, T., Ayache, N., Fischl, B., & Golland, P. Spherical demons: fast diffeomorphic landmark-free surface registration. *Medical Imaging, IEEE Transactions* **2010**, *29(3)*, 650–668.
31. Granger, S., & Pennec, X. Multi-scale EM-ICP: A fast and robust approach for surface registration. *Lecture notes in computer science* **2002**, 418–432.
32. Risser, L., Vialard, F., Wolz, R., Murgasova, M., Holm, D. D., & Rueckert, D. Simultaneous multi-scale registration using large deformation diffeomorphic metric mapping. Medical Imaging, *IEEE Transactions* **2011**, *30(10)*, 1746–1759.
33. Kircher, S., & Garland, M. Editing arbitrarily deforming surface animations. *ACM Transactions on Graphics (TOG)* **2006**, *25(3)*, 1098–1107.
34. Gu, X., Wang, Y., & Yau, S.T. Geometric compression using Riemann surface structure. *Communications in Information and Systems* **2004**, *2(3)*, 171–182.
35. Lui, L. M., Wen, C., & Gu, X. A Conformal Approach for Surface Inpainting. *AIM Inverse Problems and Imaging* **2013**, *7(3)*, 863–884.
36. Gruen, A., & Akca, D. Least squares 3D surface and curve matching. *ISPRS Journal of Photogrammetry and Remote Sensing* **2005**, *59(3)*, 151–174.